Materials Research Proceedings 44 (2024) 241-253 https://doi.org/10.21741/9781644903254-27

Contour precision controlling of welding distortion in fabrication for stainless steel hyperbolic shells adopting mechanical constraints

ZHAI Hua[1,a *], LI Cheng[1], LIU Zhihong[2], MA Jianguo[2], JI Haibiao[2], YAN Jianwen[3], LIU Qiong[3] and ZHU Xiaofeng[4]

[1]Anhui Province Key Lab of Aerospace Structural Parts Forming Technology and Equipment, Hefei University of Technology, Hefei 230009, China

[2]Institute of Plasma Physics, Chinese Academy of Sciences, Hefei 230031, China

[3]Hefei Metal Forming Intelligent Manufacturing Co., LTD, Hefei 230601, China

[4]China Institute of Atomic Energy, Beijing 102413, China

[a]jxzhaihuajx@hfut.edu.cn

Keywords: Double Shell Structure, Welding Distortion, Mechanical Constraint, Contour Precision Controlling, Inherent Strain Method

Abstract. Double-layer shell structures are widely used in the carapaces of vacuum vessels, cyclotrons, submarines and ships. The design of this double-layer structure considers the structural strength, sealing and special conditions. In the shell processing, the crisscross ribs are welded with the inner and outer shells to become parts. The welding deformation caused by multiple joints exceeds the tolerance, and external constraints are needed to ensure the forming accuracy of the contour. In this paper, the suppression effect of fixture and rigid constraint method on welding deformation of butt joint and T-joint was analyzed. The welding specimen of the double-layer shell structure was carried out, and the influence of different welding sequences on the final welding deformation was analyzed. Through external mechanical constraints, the deformation is reduced from 7.27 mm to 2.89 mm, which meets the tolerance requirements. The measured deformation is compared with the simulation results based on the inherent strain theory, which verifies the reliability of the numerical model and provides technical guidance for engineering manufacturing.

Introduction

The shell components of vacuum vessels, cyclotrons, submarines and ships are usually designed as double-layer shell structures, mainly considering strength, tightness, pressurization and special work conditions [1-2]. Due to the harsh service environment conditions, the processing accuracy, structural strength, and long-term service reliability of the double-layer shell components have high requirements. Cyclotrons and vacuum vessels in fusion reactor have a thick-walled double shell structure with intricate ribs and high-density, full-penetration welded joints [3]. The shell component is a large-scale structure with a complex hyperbolic curved shell, which usually adopts a multi-block segmented welding method. The assemble and welding of multi-block components forms the final shell components [4]. It is inevitable to cause independent block deformation and accumulate deformation in the process of continuous manufacturing. To improve the manufacturing accuracy of the shell, it is necessary to calculate and suppress the welding deformation of each manufacturing stage to ensure that the final contour precision of the shell can meet the tolerance requirements [5]. The welding deformation is positively correlated with the accumulated heat input during the welding process. Choosing reasonable welding method, welding sequence, welding parameters, and joint design can effectively reduce welding deformation. Usually, it is necessary to predict the amount of deformation through numerical simulation and then design a suitable fixture structure to suppress the generation of deformation. The finite element metho based on inherent strain has made significant achievements in predicting welding

deformation of large structures, greatly improving computational efficiency while ensuring calculation accuracy [6]. Murakawa et al. proposed the concepts of inherent strain and inherent deformation to simulate welding deformation and residual stresses [7]. Deng et al. established a finite element method to accurately simulate the welding deformation of large-scale structures considering the initial root gap [8]. Wang et al. predicted and reduced the out-of-plane welding deformation of different types of welded joints in ship panel based on inherent deformation theory [9]. Lu et al. simulated the welding deformation of T-joint using the thermo-elastic-plastic method (TEPM) and the inherent strain method (ISM), and predicted the deformation successfully of side beam of bogie using the inherent strain [10]. Zhong et al. predicted the assembly welding deformation of the 1/8 vacuum vessel using equivalent transverse and longitudinal inherent strains, and reduced the welding deformation by optimizing the welding sequence and setting constraints [11].

In addition, the design of fixture is necessary, because the external constraints can effectively reduce the welding deformation. Ma et al. investigated the welding deformation of butt joint under fixture constrained conditions through experiments. The effects of different constraint positions on longitudinal shrinkage, transverse shrinkage and angular deformation are discussed in detail [12]. Zhang et al. compared the effects of preset stiffeners and anti-deformation method on suppressing the welding deformation of 30 mm T-joints [13]. Gharib et al. studied the effects of clamping time, clamping position and heat/cold release mode on the welding deformation of butt joints [14]. Xia et al. designed a special welding fixture for the 1/16 vacuum vessel, and carried out numerical simulation and experimental measurement to verify that the welding deformation is effectively reduced [15]. Ma et al. applied the inherent deformation calculated by constrained joints to large structures to predict welding deformation controlled by jigs. The jigs near the weld are more helpful in reducing the welding deformation [16]. At present, welding deformation control of large structures with multiple welds is still challenging. The inherent strain method can be used in numerical simulation, which also means that the inherent strain of the joint needs to be calculated first. The accuracy of inherent strain directly affects the prediction results of large components. In addition, the fixture is designed according to the results of deformation prediction, which requires higher simulation accuracy, otherwise it will lead to the increase of research and development cost in the manufacturing process. The difference of different welding structure characteristics makes the welding deformation suppression scheme different. There are few research literatures on welding deformation of double-layer shell structure. In this paper, according to the characteristics of double-layer structure, the optimal welding sequence, welding deformation mechanism and welding deformation suppression are studied, which brings data support to engineering manufacturing.

In this paper, the deformation suppression of typical welded joints of double-layer shell structure was studied. The clamping constraint was used to reduce the angular deformation of the butt joint, and the stiffener was used to reduce the deformation of the T-joint. The distribution of welding deformation before and after constraint was analyzed in detail. The optimal welding sequence of the double-layer shell was studied, and the welding deformation trend and mechanism under unconstrained condition were analyzed. The constraint system was used to suppress the deformation of the double-layer shell. Finally, the deformation is controlled within the tolerance range and the results are compared with the experimental measurement.

Numerical simulation method of welding deformation

In the calculation process of the welding temperature field, a nonlinear heat transfer equation is used to describe the heat transfer process generated by the welding arc inside the welded workpiece.

Materials Research Proceedings 44 (2024) 241-253 https://doi.org/10.21741/9781644903254-27

$$\rho c\frac{\partial T}{\partial t}(x,y,z,t)=-\nabla\cdot q(x,y,z,t)+Q(x,y,z,t) \tag{1}$$

where, ρ is the density of the materials, c is the specific heat capacity, T is the current temperature, q is the heat flux vector, Q is the internal heat generation rate, x, y and z are the coordinates in the reference system, t is the time and ∇ is the spatial gradient operator.

The double ellipsoidal volume heat source is used to represent the form of welding heat input [17]. The four parameters determine the shape of the heat source, a_1 is the length of the front semi-axes in the welding direction, a_2 is the length of the rear semi-axes in the welding direction, b is the semi-axes length in the direction of weld width, c is the semi-axes length in the depth direction of the weld seam. The heat flux distribution of the front and rear parts can be expressed as follows:

$$Q_1(x,y,z,t)=\frac{6\sqrt{3}f_1\eta UI}{a_1bc\pi^{3/2}}\cdot\exp\left[-3\left(\frac{x-x_0-vt}{a_1}\right)^2-3\left(\frac{y-y_0}{b}\right)^2-3\left(\frac{z-z_0}{c}\right)^2\right] \tag{2}$$

$$Q_2(x,y,z,t)=\frac{6\sqrt{3}f_2\eta UI}{a_2bc\pi^{3/2}}\cdot\exp\left[-3\left(\frac{x-x_0-vt}{a_2}\right)^2-3\left(\frac{y-y_0}{b}\right)^2-3\left(\frac{z-z_0}{c}\right)^2\right] \tag{3}$$

where, Q_1 and Q_2 are the effective power of the heat source in the front and rear hemispheres, respectively. f_1 and f_2 are the distribution coefficients of heat flux density in the front and rear hemispheres, and f_1+f_2=2. η is heat source efficiency. x_0, y_0, and z_0 are the starting point coordinates of the welding heat source, respectively. v is the welding speed, U is the welding voltage, and I is the welding current.

In the simulation model, the convection and radiation effects between the model and the external environment are considered. The convection heat loss q_c and the radiation heat loss q_r are as follows [18]:

$$q_c=-h_c\left(T_s-T_0\right) \tag{4}$$

$$q_r=-\varepsilon\sigma\left[\left(T_s+273.15\right)^4-\left(T_0+273.15\right)^4\right] \tag{5}$$

The mechanical behavior during welding is very complex. The inherent strain theory believes that the summation of thermal strain $\varepsilon_{\text{thermal}}$, plastic strain $\varepsilon_{\text{plastic}}$, creep strain $\varepsilon_{\text{creep}}$, and phase transition strain $\varepsilon_{\text{phase}}$ after the welding process is the inherent strain, which is the source of the residual stress and deformation. The inherent strain $\varepsilon_{\text{inherent}}$ can be expressed as follows [19]:

$$\varepsilon_{\text{inherent}}=\varepsilon_{\text{plastic}}+\varepsilon_{\text{thermal}}+\varepsilon_{\text{creep}}+\varepsilon_{\text{phase}} \tag{6}$$

The magnitude and distribution of the inherent strain are mainly determined by the welding parameters, such as the types of the welded joint, welding heat source, material types, and geometric parameters. In Eq. 6, creep strain and phase transition strain are usually ignored because they are relatively small. Plastic strain is the main source of deformation. Welding distortion of a weld joint mainly including four components, longitudinal shrinkage (δ_x), transverse shrinkage (δ_y), longitudinal bending (θ_x) and transverse bending (angular distortion θ_y). The four components can be calculated using the following equation [19]:

$$\begin{cases} \delta_x = \dfrac{1}{h}\iint \varepsilon_x \mathrm{d}y\mathrm{d}z \\ \delta_y = \dfrac{1}{h}\iint \varepsilon_y \mathrm{d}y\mathrm{d}z \\ \theta_x = \dfrac{12}{h^3}\iint \varepsilon_x (z - h/2)\mathrm{d}y\mathrm{d}z \\ \theta_y = \dfrac{12}{h^3}\iint \varepsilon_y (z - h/2)\mathrm{d}y\mathrm{d}z \end{cases} \tag{7}$$

where, ε_x is the plastic strain in the welding direction (longitudinal direction), ε_y is the plastic strain in the transverse direction, h is the thickness.

The inherent deformation is obtained by integrating the plastic strain with Eq. 7, and the elastic analysis can be carried out by introducing the inherent deformation into the finite element model. The determination of the magnitude of the inherent strain depends on the prior thermo-elastic-plastic analysis. Reference [20-21] proposed an empirical method for calculating inherited strains based on extensive experimental research. Assumptions K and ξ are the longitudinal and transverse inherent strain coefficients respectively. After a lot of experiments and numerical simulations, K and ξ depend on the value of Q/h^2, as shown in Fig. 1.

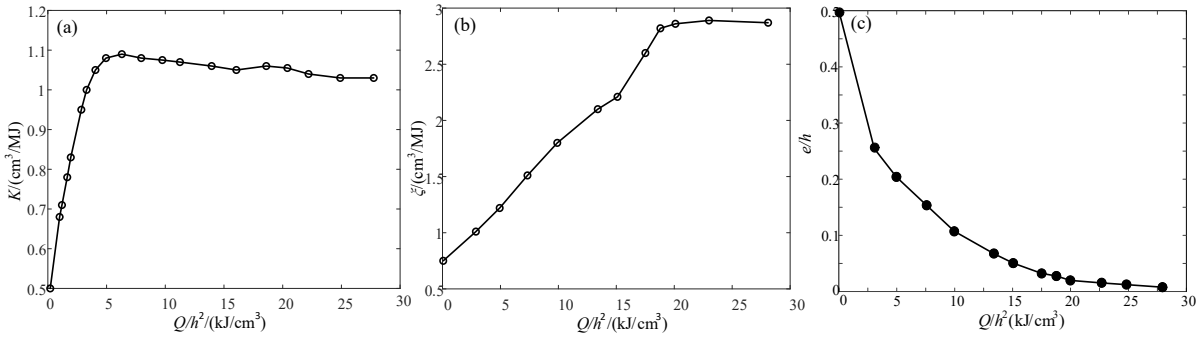

Fig. 1. The coefficient of empirical inherent strain method. (a) Longitudinal inherent strain coefficient. (b) Transverse inherent strain coefficient. (c) Eccentricity.

The magnitude range of Q/h^2 in engineering welding is 0~20 kJ/cm^3, and the magnitude range of medium and thick plates is generally 0~5 kJ/cm^3. Through linear curve fitting using the MATLAB, the approximate calculation formula can be obtained as follows:

$$K = \begin{cases} 0.08 \times \dfrac{Q}{h^2} + 0.7 & \left(\dfrac{Q}{h^2} < 5\right) \\ 1.1 & \left(\dfrac{Q}{h^2} \ldots 5\right) \end{cases} \tag{8}$$

$$\xi = \begin{cases} 0.1025 \times \dfrac{Q}{h^2} + 0.75 & \left(\dfrac{Q}{h^2} < 20\right) \\ 2.8 & \left(\dfrac{Q}{h^2} \ldots 20\right) \end{cases} \tag{9}$$

For multi-pass welding, the total volume of longitudinal inherent strain W_x and transverse inherent strain W_y can be expressed as [21]:

$$W_x = W_{xm} + 2S\varepsilon \tag{10}$$

$$W_y = \sum W_{yi} = \sum \xi_i Q_i \tag{11}$$

where, W_{xm} is the sum of longitudinal inherent strains for single pass welding; S is the area of the weld seam. ε is the yield strain. Q_i is the line energy of the i-layer weld, ξ_i is the inherent strain coefficient corresponding to the i-layer weld.

In the finite element model, the inherent strain application area can be set in the calculation model, and the anisotropy thermal expansion coefficient of the material in the inherent strain area can be defined. Unit temperature load can be applied to achieve the loading of the longitudinal and transverse inherent strains of the weld. The coefficient of thermal expansion α_x and α_y can be obtained using the following equations:

$$\alpha_x = \frac{W_x}{A\Delta T} \tag{12}$$

$$\alpha_y = \frac{W_y}{A\Delta T} \tag{13}$$

where, A is the sectional area of the inherent strain application unit; α_x corresponds to the coefficient of thermal expansion in the direction of longitudinal inherent strain, α_y corresponds to the coefficient of thermal expansion in the direction of transverse inherent strain; ΔT is the unit temperature load.

For different joint types, the applied area of inherent strain is different, as shown in Fig. 2. For butt joints, the thermal expansion coefficient can be applied to the rectangular area nearby of weld [21]:

$$A = 2a \times h' \tag{14}$$

where, a is the half-width of the natural inherent loading area, h' is the thickness of the inherent strain loading area, $h'=h-2e$, e is the eccentric value, also depending on the value of Q/h^2, as shown in Fig. 1(c).

For T-joints, the heat will be applied to the flange and web at the same time during welding, and the inherent strain shall be calculated separately. The line energy calculation of the flange and web can use the following equations [22]:

$$Q_f = \frac{2h_f}{2h_f + h_w} Q_{total} \tag{15}$$

$$Q_w = \frac{h_w}{2h_f + h_w} Q_{total} \tag{16}$$

where, Q_f and Q_w are the line energies obtained from the flange and web, respectively; h_f and h_w are the thicknesses of flange and web, respectively; Q_{total} is the total linear energy of the weld.

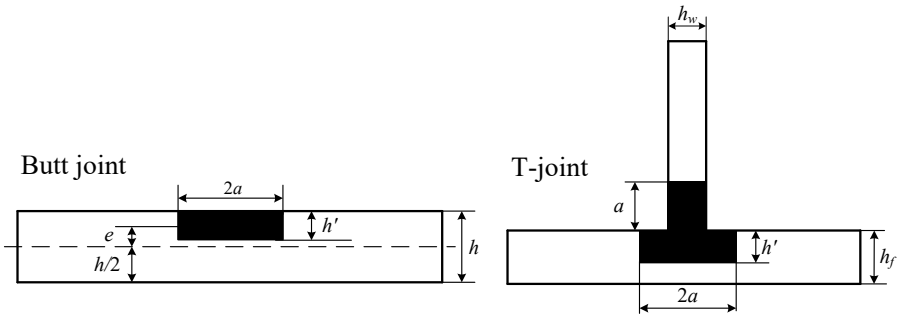

Fig. 2. Application methods of inherent strain for different joints.

Materials Research Proceedings 44 (2024) 241-253 https://doi.org/10.21741/9781644903254-27

Numerical simulation of welding deformation suppression

Double-layer shell structure and welded joints. The double-layer shell structure studied in this paper is the part of the carapace of the cyclotron, and its manufacturing accuracy will directly affect the subsequent multi-block assembly and welding. The structure is formed by welding, and the contour of the curved surface shape needs to be effectively guaranteed. The exploded view of the double-layer shell structure is shown in Fig. 3(a), which is composed of the outer shell, inner shells, toroidal ribs, and poloidal ribs, mainly including X-groove butt joint, double V-groove T-joints, and J-groove T-joints. To be more specific, the welding between inner shells is a X-groove butt joint. The welding between inner shells and ribs is double V-groove T-joints. The welding between ribs is double V-groove T-joints. The welding between the outer shell and ribs is J-groove T-joints, as shown in Fig. 3(b)-(d).

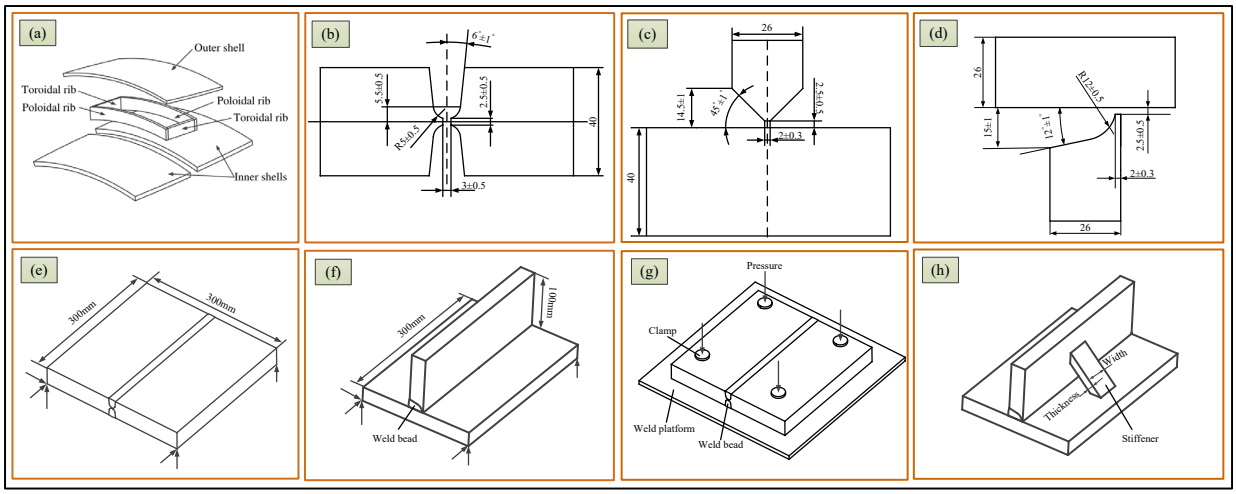

Fig. 3. Double shell structure and different welded joint: (a) Double shell structure, (b) X groove butt joint, (c) K groove T-joint, (d)J groove T-joint, (e) Unconstrained butt joint, (f) Unconstrained T-joint, (g) Restraint conditions of butt joint, (h) Restraint conditions of T-joint.

The typical joints of the shell structure are numerically simulated, and the influence of different constraints on the welding deformation is analyzed. The mitigation of deformation was the major focus of this work, and different constraint schemes were constructed utilizing the mechanical constraints. The first is the free state, which is bounded by three corners, as shown in Fig. 3(e)-(f). It is a necessary limitation to prevent inaccurate spatial motion trends. The butt joint is constrained by the clamping mechanism, and the T-joint is constrained by the reinforcing rib, as shown in Fig. 3(g)-(h). Considering the interaction between the fixture and the sample, the simulation model of the constraint fixture is established. To accurately simulate the thermodynamic behavior during the welding process, temperature-dependent material properties were used. The base metal is 304 stainless steel, and the welding wire is ER316. It is assumed that the material parameters of the welding material are the same as those of the base metal. The manual gas tungsten arc welding method was used to conduct experiments on welding joints to evaluate the reliability of the welding process. The welding process parameters are shown in Tab.1. In the multi-layer welding process, the interlayer temperature is controlled below 150°C.

Table 1. Welding parameters of the manual TIG welding.

Type	X-groove	K-groove	J-groove
Welding pass	20-25	12-15	12-15
Welding voltage (U/V)	8-12	9-12	8-12
Welding current (I/A)	125-220	160-293	150-274
Welding speed (v/mm·min^{-1})	80-120	80-120	80-360

Welding deformation suppression of butt joint. The out of plane deformation of butt joint after welding are shown in the Fig. 4. The results of welding deformation without constraints are shown in Fig. 4(a), from which the welding deformation in the vertical direction has a certain symmetry. It can be found that the transverse inherent strain has a greater effect on the welding deformation, resulting in an overall V-shaped deformation. The welding deformation constrained by the clamping mechanism is shown in Fig. 4(b). Due to the constraint of the welding platform, the deformation of the weld center is reduced, and the angular shrinking causes both ends being upward. In the free state, both sides of the edge by the initial restraint, the center region deformation to the downside, when set the restraint, the deformation to the bottom is significantly reduced, but the sides tend to upward deformation. Under the pressure constraint of the clamping mechanism, the out-of-plane deformation is obviously alleviated. Fig. 4(c) compares the distribution of welding deformation in the vertical direction, and with the application of constraints, the deformation of the weld joint decreases. The restraint scheme reduces out of plane deformation by 38.6%.

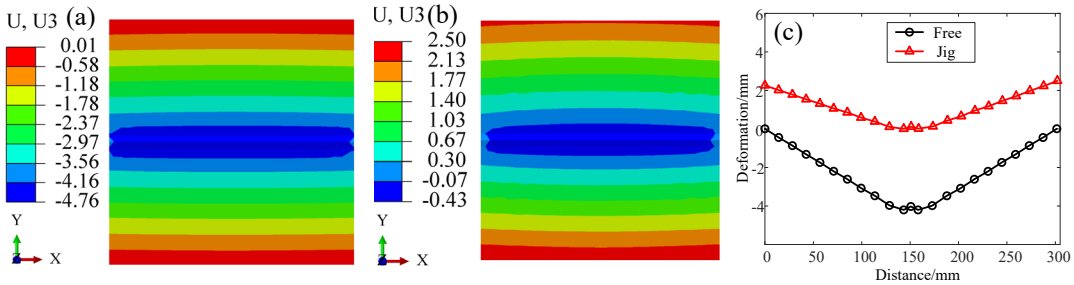

Fig. 4. Welding deformation simulation of butt joint. (a) Unconstrained state. (b) Restrained condition. (c) Comparison of angular deformation.

Welding deformation suppression of T-joint. The welding deformation of T-joint are shown in the Fig. 5. The result of welding deformation without constraint is shown in Fig. 5(a). Due to the boundary condition, edge region of the flange plate was fixed with almost none deflection, web plate bend downward with about 34.7 mm magnitude of welding angular distortion. The deformation result with stiffener is shown in Fig. 5(b). The stiffeners play a structural constraint role, which hinders the deformation trend and significantly reduces the welding deformation. The welding angle deformation of the web is reduced to 3.7 mm. This means that the structural constraints of the stiffeners reduce the welding deformation by 89.3 %. It can be determined that external mechanical constraints can significantly inhibit welding deformation.

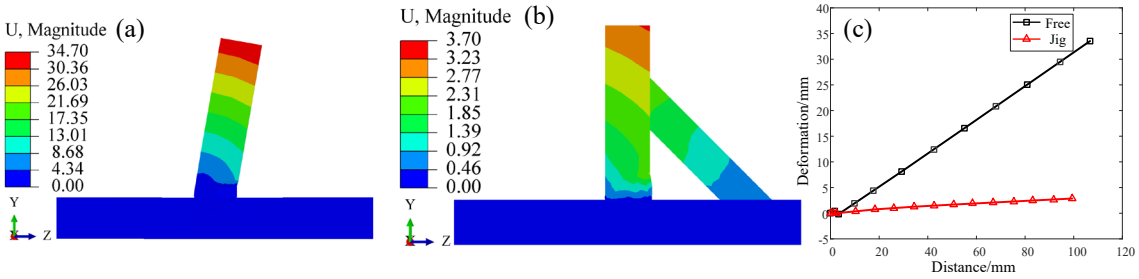

Fig. 5. Welding deformation simulation of T-joint: (a) Unconstrained state, (b) Restrained condition, (c) Comparison of angular deformation.

Welding deformation suppression of double-layer shell structure

Optimum welding sequence. The double-layer shell structure has multiple welded joints, and the welding sequence has a certain influence on the final welding deformation. The inner shell is the carrier of welding, so the first step is to weld the inner shell, then weld the four ribs on the inner shell, and finally weld the outer shell. According to the characteristics of the structure, we have developed the following possible welding sequences, as shown in Fig. 6. The welding of the outer shell has a variety of possibilities because it is a square weld, so it is necessary to analyze the influence of different welding sequences on the deformation of the outer shell. Four welding cases are designed and the optimum welding sequence should be analyzed.

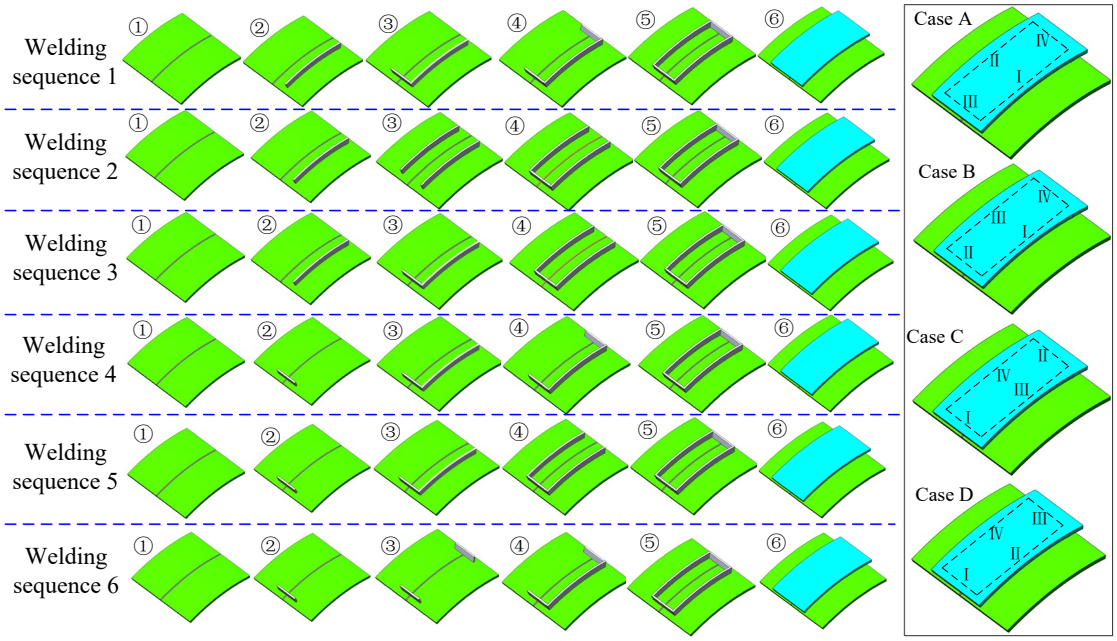

Fig. 6. Design of different welding sequences.

In the numerical simulation analysis, in order to simulate the spot welding constraint in the welding experiment, four nodes are taken at both ends of the inner shell for constraint. Without other mechanical constraints, the welding deformation under unconstrained conditions is discussed. The parts are gradually added to the model according to the welding sequence, and the activation sequence is defined by the birth-death element. The welding sequence 1 and Case A simulation results in Fig. 6 are shown in Fig. 7, and the maximum deformation is 7.25 mm. When welding the inner shell, due to the shrinkage of the weld, the two sides are deformed upward. Then, four ribs are welded subsequently, which has little effect on the deformation of the inner shell. In addition, the maximum deformation of the longitudinal and transverse ribs is 4.2 mm and 3.9 mm. After welding, the outer shell deforms downward, with the maximum deformation of 6.15 mm.

The deformation in the middle area is the smallest, due to the mechanical interaction between the surrounding welds. From the deformation results, this is far beyond the tolerance requirements, so it is necessary to suppress the welding deformation.

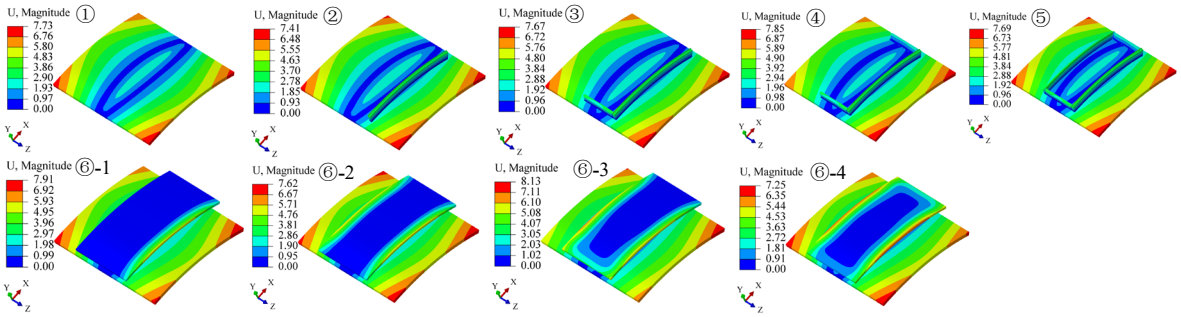

Fig. 7. Welding deformation results according to the welding sequence 1.

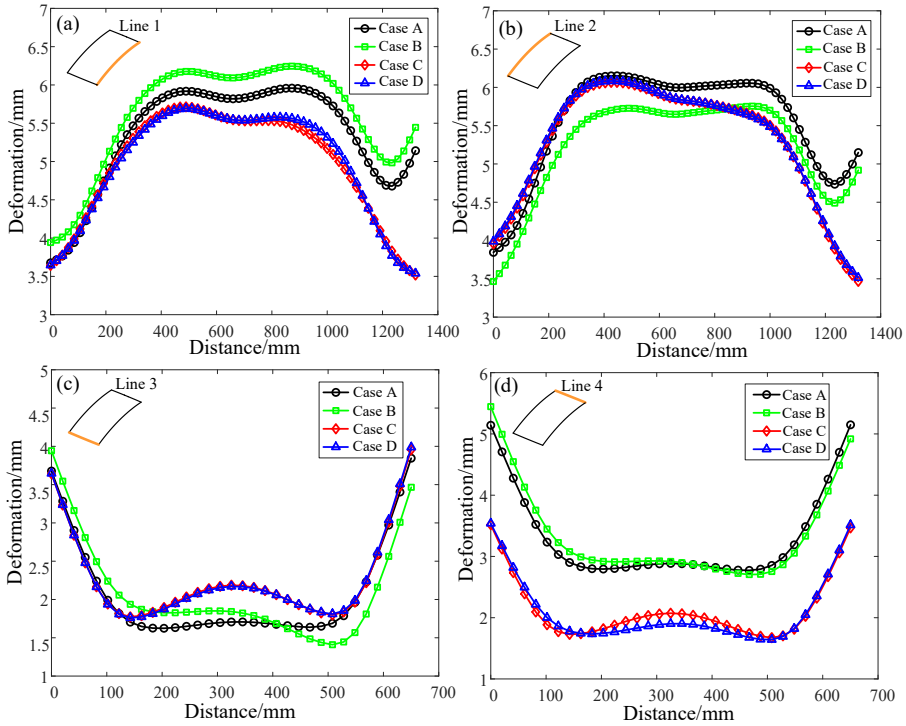

Fig. 8. Welding deformation of different lines of the outer shell: (a) Line 1, (b) Line 2, (c) Line 3, (d) Line 4.

As the weld bead is welded one by one, the stiffness of the weldment will change, and the shrinkage of the post weld bead will be constrained by the structure. The welding deformation of outer shell in Case A, Case B, Case C and Case D needs to be discussed in detail. Based on the welding sequence 1, the influence of different welding schemes on the deformation of the outer shell is analyzed by numerical simulation. Four lines were selected to compare the difference of welding deformation, as shown in Fig. 8. In summary, welding deformation of Case C and Case D is smaller than that of Case A and Case B. This is because Case C and Case D first weld short ribs to produce structural constraints, which reduces the deformation during subsequent welding of long ribs. Because of the stronger shrinkage tendency, the average deformation of the long ribs is obviously greater than that of the short ribs. In addition, the first welded rib always deforms significantly because it is more prone to deformation without the constraints of other ribs. After comparison, it can be found that Case C is the optimum sequence for welding the outer shell, that is, short ribs are first welded and than welding long ribs.

It has been determined that the welding scheme of Case C is adopted in the overall welding sequence. The numerical simulation process of welding deformation of different welding sequences in Fig. 6 is shown in Fig. 9. In the six welding sequences, the first step is to weld the inner shell, but the difference produced from the second step, which also leads to the difference of the final welding deformation. In summary, the maximum deformation is 7.40 mm and the minimum deformation is 7.27 mm in the six welding sequence. It can be concluded that the welding sequence has no obvious effect on the maximum deformation of the double-layer frame structure.

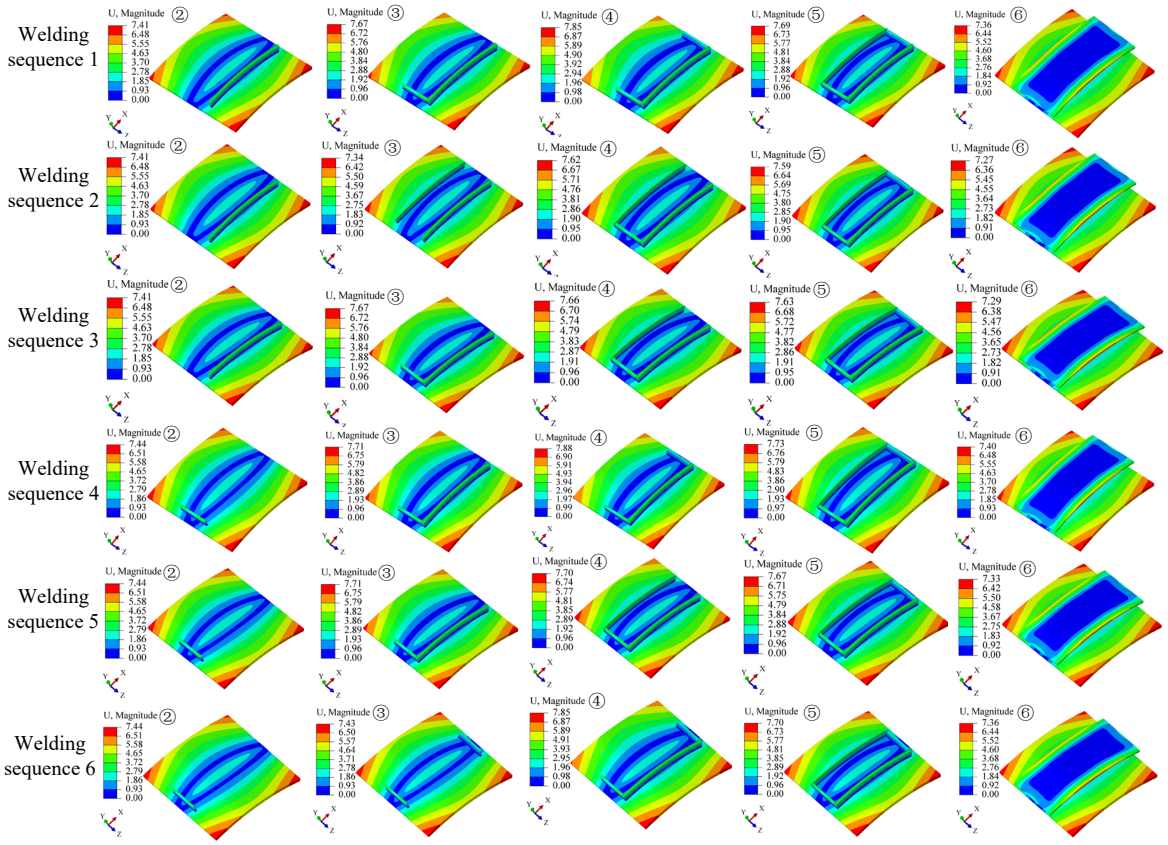

Fig. 9. Welding deformation under different welding sequences.

Welding deformation suppression. In the previous content, the method of suppressing welding deformation was studied. The external pressure is used to limit the deformation in the butt joint, and the stiffener is used to constrain the deformation in the T-joint. According to the mechanical constraints used in processing and converted into corresponding load in simulation. Specifically, when welding the inner shell, an external load is applied to suppress the deformation. When welding four ribs, the stiffeners are set to limit the deformation. When welding the outer shell, anti-deformation back ribs are applied to its back to resist the shrinkage. According to the unconstrained state, the deformation of the welding sequence 2 is the smallest, so the deformation is suppressed in accordance following the order. The welding deformation suppression results are shown in Fig. 10. Finally, The maximum deformation is is reduced to 2.89 mm.

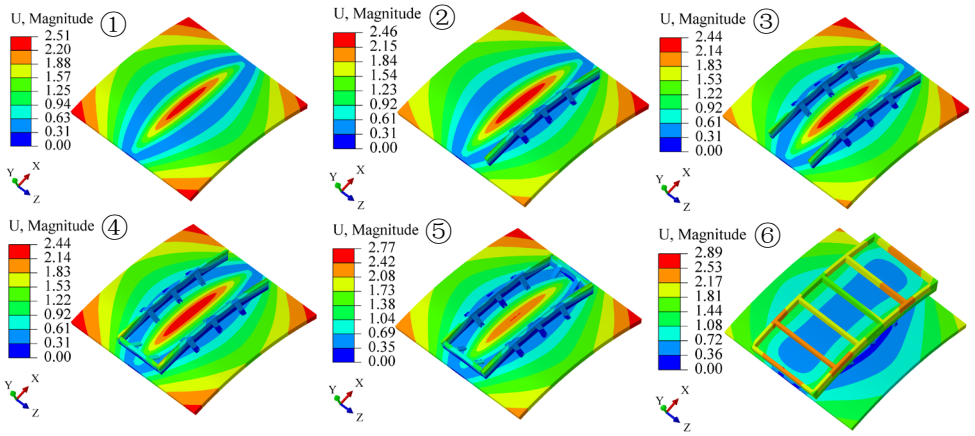

Fig. 10. Welding deformation suppression results following the welding sequence 2.

Welding experiment. The Jigs system in the numerical simulation process was manufactured for actual welding. Jigs were used to restrict welding distortion in all welding processes and add and remove the fixture in the appropriate process. Bolt clamping mechanisms were arranged around the inner shells, and stiffeners were used to fix ribs on the inner shells during welding. Finally, anti-deformation back ribs were used to reduce the deformation of the outer shell. The trend and magnitude of welding deformation were measured after welding. The double shell welded weldment is shown in Fig.11(a). The numerical calculation and experimental measurement results were compared, as shown in Fig. 11(b) and (c), which shows that the results of both are highly consistent. The deformation of numerical simulation is small because the jigs are fixed by spot welding for easy removal, so the degree of restraint is lower than that of numerical simulation.

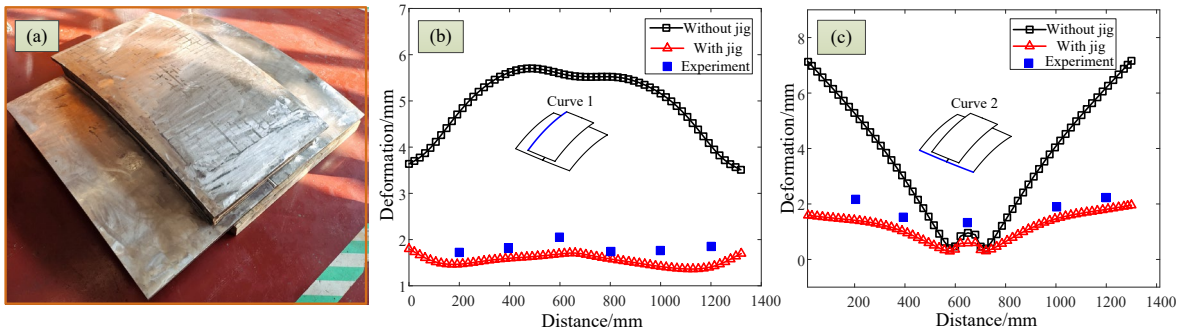

Fig. 11. Welding deformation suppression results: (a) Processed weldment, (b) Deformation of curve 1, (c) Deformation of curve 2.

Conclusions

In this paper, based on the inherent strain method, the welding deformation distribution of butt joints and T-joints is numerically simulated, and the influence of constraint schemes on the suppression of welding deformation is compared. Finally, the experimental study and numerical simulation of the welding deformation and its mitigation of the double-layer shell structure were conducted. The main conclusions are as follows:

(1) Numerical simulation models of welding deformation of butt joints and T-joints were established. Under the constraint scheme, the angular deformation of the butt joint is reduced by 38.6 %, and the angular deformation of the T-joint is reduced by 89.3 %, which verifies the effectiveness of the mechanical constraint to suppress the welding deformation.

(2) Six overall welding sequences of double-layer shell structure and four welding schemes of outer shell are designed. The distribution law of welding deformation is compared, and welding sequence 2 and Case C are determined as the optimum welding sequence.

(3) A jig system was designed to suppress the welding deformation of the double-layer shell structure, and the welding experiment was carried out. The influence of fixture on welding deformation distribution was analyzed. The maximum welding deformation was reduced from 7.27 mm down to 2.89 mm. The numerical simulation results are compared with the deformation experimental measurements, which verifies the effectiveness and provides guidance for engineering manufacturing.

Acknowledgements
The experimental part of this paper is supported by the Institute of plasma physics, Chinese academy of sciences and Hefei metal forming intelligent manufacturing Co., LTD. This work was supported by Anhui Province Key Project No. 202103a07020010, and No. 202304a05020074, flexible molding equipment for carbon fiber composite materials, JZ2023GQBK0070.

References

[1] Y.T. Kim, T.J. Kim, T.Y. Park, C.D. Jang, Welding distortion analysis of hull blocks using equivalent load method based on inherent strain, J. Ship Res. 56 (2012) 63-70. https://doi.org/10.5957/jsr.2012.56.2.63

[2] L. Xiu, J. Wu, Z. Liu, J. Ma, X. Fan, H. Ji, X. Xia, Y. Li, Weld distortion prediction of the CFETR vacuum vessel by inherent strain theory, Fusion Eng. Des. 121 (2017) 43-49. https://doi.org/10.1016/j.fusengdes.2017.03.175

[3] H. Ji, J. Wu, H. Wu, Z. Liu, J. Ma, X. Fan, Analysis of welding deformation on CFETR 1/32 vacuum vessel mockup, Fusion Eng. Des. 144 (2019) 160-163. https://doi.org/10.1016/j.fusengdes.2019.05.012

[4] Y. Kim, J. Kim, S. Kang, A study on welding deformation prediction for ship blocks using the equivalent strain method based on inherent strain, Appl. Sci. 9 (2019) 4906. https://doi.org/10.3390/app9224906

[5] J. Yi, J. Lin, Z. Chen, T. Chen, Prediction and controlling for welding deformation of propeller base structure, J. Ocean. Eng. Sci. 6 (2021) 410-416. https://doi.org/10.1016/j.joes.2021.06.002

[6] H. Murakawa, Y. Luo, Y. Ueda, Prediction of welding deformation and residual stress by elastic FEM based on inherent strain (first report) mechanism of inherent strain production, J. Soc. Nav. Archit. Jpn. 180 (1996), 739-751. https://doi.org/10.2534/JJASNAOE1968.1998.323

[7] H. Murakawa, D. Deng, N. Ma, Concept of inherent strain, inherent stress, inherent deformation and inherent force for prediction of welding distortion and residual stress, Trans. J.W.R.I. 39 (2010) 103-105. https://www.semanticscholar.org

[8] D. Deng, H. Murakawa, W. Liang, Numerical simulation of welding distortion in large structures. Comput. Methods Appl. Mech. Eng. 196 (2007) 4613-4627. https://doi.org/10.1016/j.cma.2007.05.023

[9] J. Wang, S. Rashed, H. Murakawa, Y. Luo, Numerical prediction and mitigation of out-of-plane welding distortion in ship panel structure by elastic FE analysis, Mar. Struct. 34 (2013) 135-155. https://doi.org/10.1016/j.marstruc.2013.09.003

[10] Y. Lu, C. Lu, D. Zhang, T. Chen, J. Zeng, P. Wu, Numerical computation methods of welding deformation and their application in bogie frame for high-speed trains, J. Manuf. Process. 38 (2019) 204-213. https://doi.org/10.1016/j.jmapro.2019.01.013

[11] Y. Zhong, Z. Liu, J. Wu, J. Ma, J. Tao, H. Ji, Optimization of welding distortion of vacuum vessel for nuclear fusion based on finite element analysis, Fusion Eng. Des.195 (2023) 113935. https://doi.org/10.1016/j.fusengdes.2023.113935

[12] N. Ma, H. Huang and H. Murakawa, Effect of jig constraint position and pitch on welding deformation, J. Mater. Process. Technol. 221 (2015) 154-162. https://doi.org/10.1016/j.jmatprotec.2015.02.022

[13] C. Zhang, S. Li, J. Sun, Y. Wang, D. Deng, Controlling angular distortion in high strength low alloy steel thick-plate T-joints, J. Mater. Process. Technol. 267 (2019) 257-267. https://doi.org/10.1016/j.jmatprotec.2018.12.023

[14] A.R. Gharib, F.R. Biglari, M. Shafaie, A.H. Kokabi, Experimental and numerical investigation of fixture time on distortion of welded part, Int. J. Adv. Manuf. Technol. 104 (2019) 1121-1131. https://doi.org/10.1007/s00170-019-03874-0

[15] X. Xia, H. Ji, J. Wu, H. Wu, Z. Liu, J. Ma, X. Fan, Research on welding deformation of CFETR 1/16 vacuum vessel mockup, Fusion Eng. Des. 151 (2020) 111411. https://doi.org/10.1016/j.fusengdes.2019.111411

[16] N. Ma, H. Huang, Efficient simulation of welding distortion in large structures and its reduction by jig constraints, J. Mater. Eng. Perform. 26 (2017) 5206-5216. https: //doi.org/10.1007/s11665-017-3000-4

[17] J. Goldak, A. Chakravarti, M. Bibby, A new finite element model for welding heat sources, Metal. Trans. B. 15 (1984) 299-305. https://link.springer.com/article/10.1007/BF02667333

[18] G. Fu, M.I. Lourenço, M. Duan, S.F. Estefen, Influence of the welding sequence on residual stress and distortion of fillet welded structures, Mar. Struct. 46 (2016) 30-55. https://doi.org/10.1016/j.marstruc.2015.12.001

[19] D. Deng, H. Murakawa, Prediction of welding distortion and residual stress in a thin plate butt-welded joint, Comput. Mater. Sci. 43 (2008) 353-365. https://doi.org/10.1016/j.commatsci.2007.12.006

[20] J. Xu, L. Chen, J. Wang, C. Ni, Prediction of welding distortion in multipass girth-butt welded pipes of different wall thickness, Int. J. Adv. Manuf. Technol. 35 (2008) 987-993. https://doi.org/10.1007/s00170-006-0782-1

[21] J. Wang, H. Lu, Prediction of welding deformations by FEM based on inherent strains, J Shanghai Jiaotong Univ. 2 (2000) 83-87. https://www.semanticscholar.org

[22] W. Liang, D. Deng, Influences of heat input, welding sequence and external restraint on twisting distortion in an asymmetrical curved stiffened panel, Adv. Eng. Softw. 115 (2018) 439-451. https://doi.org/10.1016/j.advengsoft.2017.11.002